*Progress In Electromagnetics Research B, Vol. 78, 143–154, 2017*

# Accurate Determination of Gold Nanorods Concentrations from Optoacoustic Signals Detected at 870 nm and 905 nm by Using High-Power Diode Lasers with Fast Switching Electronics

**Luca Leggio*, Daniel Gallego, Raul Arroyo, Sandeep B. Gawali, Sergio Rodríguez, Miguel Sánchez, Guillermo Carpintero, and Horacio Lamela**

**Abstract**—Optoacoustic imaging (OAI) is an emerging biomedical technique that allows visualization of in-depth tissues by using ultrasonic signals generated by short laser pulses. In this work, the authors combine the optical power of several pulsed high-power diode lasers (HPDLs) at 870 nm and 905 nm to a 7-to-1 675-μm fiber bundle to generate optoacoustic (OA) signals from different mixtures of two gold nanorods solutions with absorbance peak at ∼ 860 nm and ∼ 900 nm, respectively. The pulses produced to generate OA signals are alternated between the two wavelengths by a microcontroller circuit with fast switching (0.5 ms). From the amplitude of the OA signals, the concentrations of the nanoparticles solutions are easily estimated with high accuracy using a fluence model. The results achieved with the proposed system show very good agreement between the concentrations of gold nanorods estimated from measurements and the expected values.

## 1. INTRODUCTION

OAI is an emerging modality of biomedical imaging for visualization of soft tissues with high resolution. It is based on the detection of ultrasonic waves generated by the irradiation and absorption of short pulses of light by a biological tissue. The endogenous or exogenous chromophores contained in the tissue absorb the pulsed light that produces a transient raise of the local temperature from the conversion of the electromagnetic energy into heat. Then, the consequent thermoelastic expansion causes a pressure increase that is followed by the emission of broadband OA waves. These ultrasonic waves convey the information about the absorption map, i.e., the size and shape of the chromophores distribution contained in the tissue [1]. Generally, an array of ultrasonic transducers around the tissue converts the ultrasonic waves into electrical signals, which are collected to form an image by using a reconstruction algorithm. OAI combines the high contrast of the optical techniques with the high resolution of the ultrasonic imaging, since the acoustic scattering is at least two orders of magnitude lower than optical scattering in biological soft tissues. OAI allows higher penetration depth and higher spatial resolution than optical imaging techniques such as diffuse optical tomography and fluorescence tomography [2].

Unlike X-ray, OAI uses non-ionizing radiation in the biological window (600–1300 nm), where the optical absorption of the biological tissues is much higher than the scattering [3]. The relevant characteristics of the light source for OAI are: the pulse width (ns), the repetition frequency (several Hz), the pulse energy (mJ), the emission wavelength (in near infrared) and the beam profile. In order to efficiently generate OA signals, the tissue is irradiated with short pulses to satisfy the conditions of thermal and stress confinement [4]. To achieve the condition of thermal confinement, the heat

*Received 8 August 2017, Accepted 17 September 2017, Scheduled 25 September 2017*

* Corresponding author: Luca Leggio (lleggio@ing.uc3m.es).

The authors are with the Department of Electronics Technology, Optoelectronic and Laser Technology Group (GOTL), University Carlos III of Madrid, Av. de la Universidad, 30, Leganés 28911, Spain.

diffusion in the irradiated volume should be negligible during the excitation pulse. More restrictive is the condition of stress confinement that requires pulse durations shorter than the transit time for an acoustic wave to pass through the irradiated volume. For instance, to achieve a resolution of 150 μm, a pulsed laser source capable of pulse width durations of 100 ns or shorter is required. Under these conditions, the initial pressure is proportional to the absorbed energy density [5]. A laser source with a high repetition frequency is advantageous when the OA application involves scanning or uses signal averaging for increasing the signal to noise ratio, since it reduces the total amount of acquisition time spent. The energy per pulse required depends greatly on the illuminated area and the penetration depth required by the actual application of an OA system. The maximum energy density applicable to a biological tissue is limited to 20 mJ/cm$^2$ by ANSI safety standard. The capability of selecting a specific wavelength in the biological window for the light source is a very attractive feature for the quantification of chromophores in OA spectroscopy (OAS). The emission wavelength used depends on the kind of absorber targeted. The typical laser sources used for OAI are solid state lasers, tunable dye lasers, and optical parametric amplifiers [6, 7]. These sources can provide pulses with energy from several tens of μJ to hundreds of mJ, with duration of several ns. However, their use for clinical applications is limited by their low repetition rates in the range of tens of Hz, the high cost and the bulky size that are mainly due to the power supply and cooling elements [8]. On the other hand, HPDLs [9–11] could be an alternative to overcome all these limitations of solid state lasers for OAI, due to their small size, low cost, availability in a wide range of near-infrared (NIR) wavelengths [12–15], and high repetition rates (kHz) for a fast signal acquisition [16, 17]. Although HPDLs offer several advantages compared to other lasers, their output power is relatively low. The energy per pulse is limited to a few tens of μJ, due to the possibility of catastrophic degradation of end facets [18]. A possible solution to this problem is to efficiently combine the output optical power of several HPDLs via optical lenses and fibers [19]. To reach the energy levels of solid state lasers, the light beam of a big amount of HPDLs should be combined. In this regard, diode laser bars (DLBs) and stacks (DLSs) could be used as a valid alternative to HPDLs, but their employment is not resolved here. In any case, if the objective is to achieve OAI of small areas of tissue, the researchers can use HPDLs in order to achieve high levels of optical fluence able to penetrate in depth.

Previous works [20, 21] reported inversion algorithms to determine the single chromophores concentrations from multi-wavelength OA images acquired. Particularly, the variations in hemoglobin oxygen saturation ($SO_2$) in single subcutaneous vessels of rats in vivo have been investigated under three physiological states: hyperoxia, normoxia, and hypoxia. The determination of chromophore concentrations (i.e., deoxyhemoglobin and oxyhemoglobin) from skin is crucial to get information about some physiological parameters contained in the blood. Deviations from the standard values of the concentrations may indicate pathologies. Similarly, absorbing solutions of copper and nickel chloride have been submerged in a phantom at different ratios to determine their concentrations from the OA images acquired at wavelengths between 590 nm and 980 nm [22]. In these works, the concentrations of the single chromophores have been estimated from the imaged map of local optical energy deposition, which is roughly proportional to the amplitude of OA signals detected. In this paper, OA signals are generated from mixed solutions of gold nanorods with absorption peaks at $\sim$ 860 nm and $\sim$ 900 nm by using two triplets of 870-nm and 905-nm HPDLs as light sources. The HPDLs beams are coupled into multimode optical fibers with core diameter of 200 μm and collected in a 7-to-1 675-μm fiber bundle. A microcontroller circuit generates alternate pulses between the two wavelengths with fast switching of 0.5 ms. This work demonstrates that the fast wavelength switching provided by the microcontroller is fundamental to obtain the concentrations of the gold nanorods solutions with high accuracy.

### 1.1. Scope of the Paper

The purpose of this paper is to estimate the concentrations of some mixtures of gold nanorods solutions, selected as potential contrast agents in a real OA application, with fast wavelength switching from the total 1-D OA signal achieved. The gold nanorods tuned to specific wavelengths could be bio-conjugated to target some kind of cells or molecules. The measured OA signals are related to the nanoparticles concentrations by using a fluence model [23]. This model is based on the approximation of the fluence distribution. It is assumed that the propagating media (i.e., the cuvette and the gold nanorods) are non-scattering media. Three mixtures of gold nanorods with different proportions are considered: 40/60,

50/50, and 60/40. From the analysis of the OA signals detected the authors are able to estimate the concentrations of the gold nanorods solutions. Results show good agreement between estimated and expected values with a maximum observational error of 2.76%. The gold nanorods proposed in this paper belong to a class of nontoxic and biocompatible nanoparticles considered as appropriate candidates for intravenous biomedical applications directed to the detection of diseases, such as cancer and arteriosclerotic plaques [24–27].

### 1.2. Layout of the Paper

The paper is organized as follows. Section 2 gives a detailed description of the OA system and the implemented diode laser sources. Section 3 describes the characteristics of the gold nanorods used in the successive experiments and introduces the inverse algorithm to estimate their concentrations from detected OA signals. Section 4 discusses the results showing the estimation of the relative concentrations.

## 2. MEASUREMENT SETUP

In this section, the OA setup used in the experiments is introduced describing the characteristics of each single element. The description of the system is divided into two blocks; the first one describes the HPDLs, the optics and the electronics, while the second one discusses the OA signal generation, detection and visualization.

### 2.1. Laser Sources, Optical Elements and Electronics

Considering the advantages of HPDLs over conventional solid-state lasers, the authors built an experimental setup operating at two different wavelengths to measure the OA signals. The excitation system is composed of two triplets of pulsed HPDLs combined side-by-side: one with central wavelength at 870 nm (L11348-330-04, Hamamatsu Photonics K.K.) and the other one at 905 nm (SPL PL90_3, OSRAM Opto Semiconductors GmbH), driven individually by diode laser drivers (PCO-7120, IXYS Colorado). Table 1 summarizes the characteristics of the HPDLs used in the experiments. Each HPDL output is separately coupled into a 200-µm multimode optical fiber (FT200EMT, Thorlabs Inc.) with a numerical aperture (N.A.) of 0.39, as shown in Fig. 1(a). The optical fibers are joined together forming a fiber bundle built in-house, composed of seven optical fibers disposed in hexagonal configuration and with an output diameter of 675-µm, as shown in Figs. 1(b) and (c). Individual lens systems formed by a collimating lens (aspheric, N.A. = 0.40, effective focal length $f_{\mathrm{EFL1}} = 6.24\,\mathrm{mm}$, material: H-LAK54) and a focusing lens (aspheric, N.A. = 0.68, $f_{\mathrm{EFL2}} = 3.1\,\mathrm{mm}$, material: H-LAK54) with anti-reflecting coatings (600–1050 nm) are used to couple the light emitted by each HPDL into the optical fibers using a 3-axis translation mount (CXYZ05, Thorlabs Inc.) to ensure optimum alignment (Fig. 1(d)). With this coupling arrangement, a magnification $M_1 = f_{\mathrm{EFL2}}/f_{\mathrm{EFL1}} \approx 0.5$ in both axes is achieved.

**Table 1.** Characteristics of the 870-nm and 905-nm HPDLs.

| Characteristics | 870-nm HPDL | 905-nm HPDL |
|---|---|---|
| Peak power (max) | 90 W | 90 W |
| Pulse width (max) | 100 ns | 100 ns |
| Duty cycle (max) | 0.075% | 0.1% |
| Aperture size | 300 µm × 10 µm | 200 µm × 10 µm |
| Divergence angles | 10°, 24° | 9°, 25° |

In order to maximize the throughput of the system reducing the total amount of time required for a multispectral measurement, the emissions of pulses at different wavelengths are time-division multiplexed whereas the emissions at the same wavelength are combined. Each HPDL has its own pulse current laser driver that is activated following a sequence generated by a trigger generator. This is

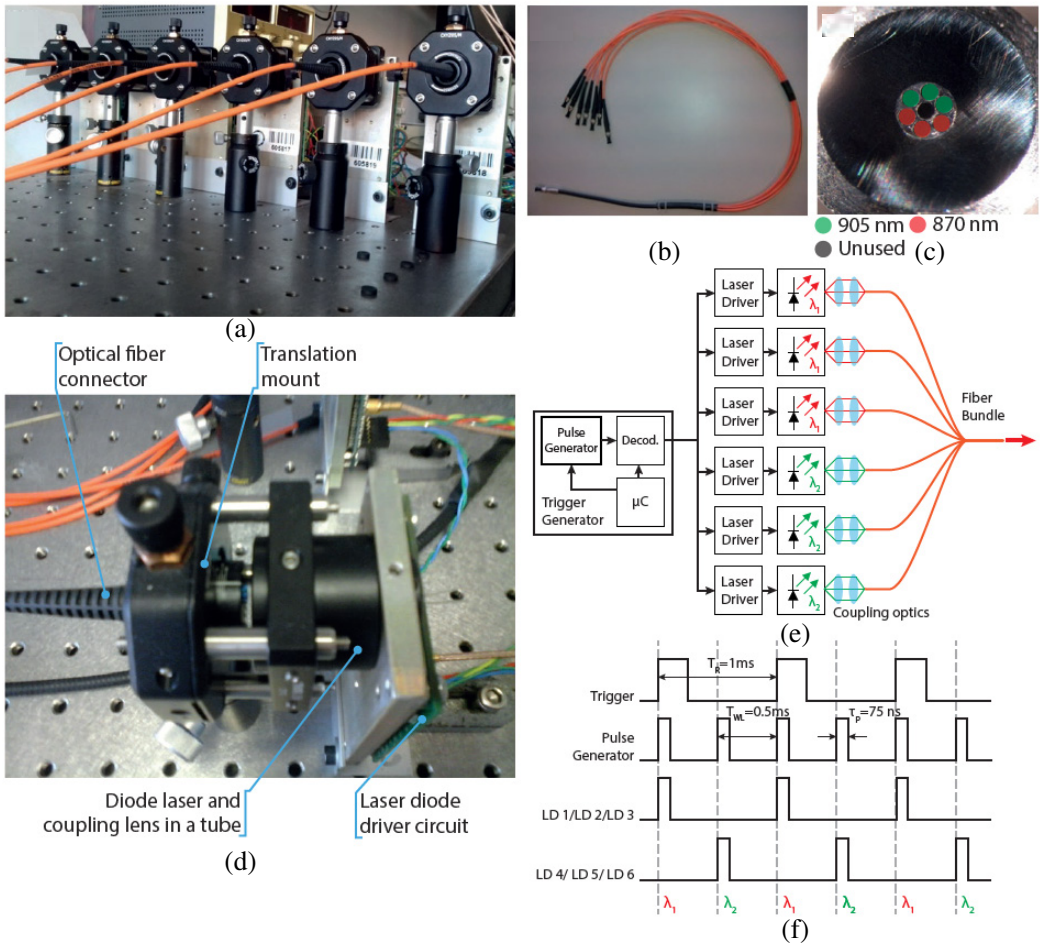


**Figure 1.** OA setup described in some pictures: (a) side-by-side beam coupling of six HPDLs into the optical fibers; (b) 675-µm fiber bundle composed of seven 200-µm optical fibers before being mounted; (c) output of the fiber bundle seen under the microscope (the positions of the optical fibers are symmetrical between the two wavelengths to ensure uniform illumination of the sample); (d) three-axial translator used to optimize the beam coupling of each HPDL into the optical fiber; (e) block diagram of the OA system with light delivery in a fiber bundle; (f) time diagram of the trigger system that shows how the pulses are alternated between the two wavelengths $\lambda_1$ and $\lambda_2$. The novelty of this design is represented by a fast acquisition of the OA signals by switching the two wavelengths with the microcontroller.

composed of a microcontroller (µC), a pulse generator, and a decoder (Fig. 1(e)). The microcontroller (pic32MX250F128B, Microchip Technology Inc., Fig. 2) triggers the pulse generator at some defined periods, $T_{WL}$, meanwhile it controls the pulse width. Through the decoder the pulse is distributed to the laser drivers up to seven drivers following a flexible programmed sequence that can be adapted to different configurations (Fig. 1(f)). The HPDLs with the same emission wavelength are activated at the same time. The minimum period between wavelengths is limited by the extinction of the acoustic wave to avoid overlapping. The period of the cycle over all wavelengths, $T_R$, should be equal or larger than the number of wavelengths times, $N$, the repetition period $T_{WL}$ ($T_R \geq N * T_{WL}$). Additionally, it cannot be lower than the minimum repetition period of the HPDLs that depends on the duty cycle ($D$) and the pulse width $\tau_p$. In this implementation the authors set a repetition period of $T_R = 1\,\text{ms}$ and a pulse width $\tau_p$ of 75 ns ($D = 0.0075\%$), and a $T_{WL}$ of 0.5 ms, which corresponds to the switching time between the two wavelengths. The microcontroller cannot be employed alone, but necessitates additional electronic elements to generate nanosecond pulses with small rise and fall times and with the appropriate amplitude to open the MOSFET of the diode laser drivers. Fig. 2 shows the circuit board

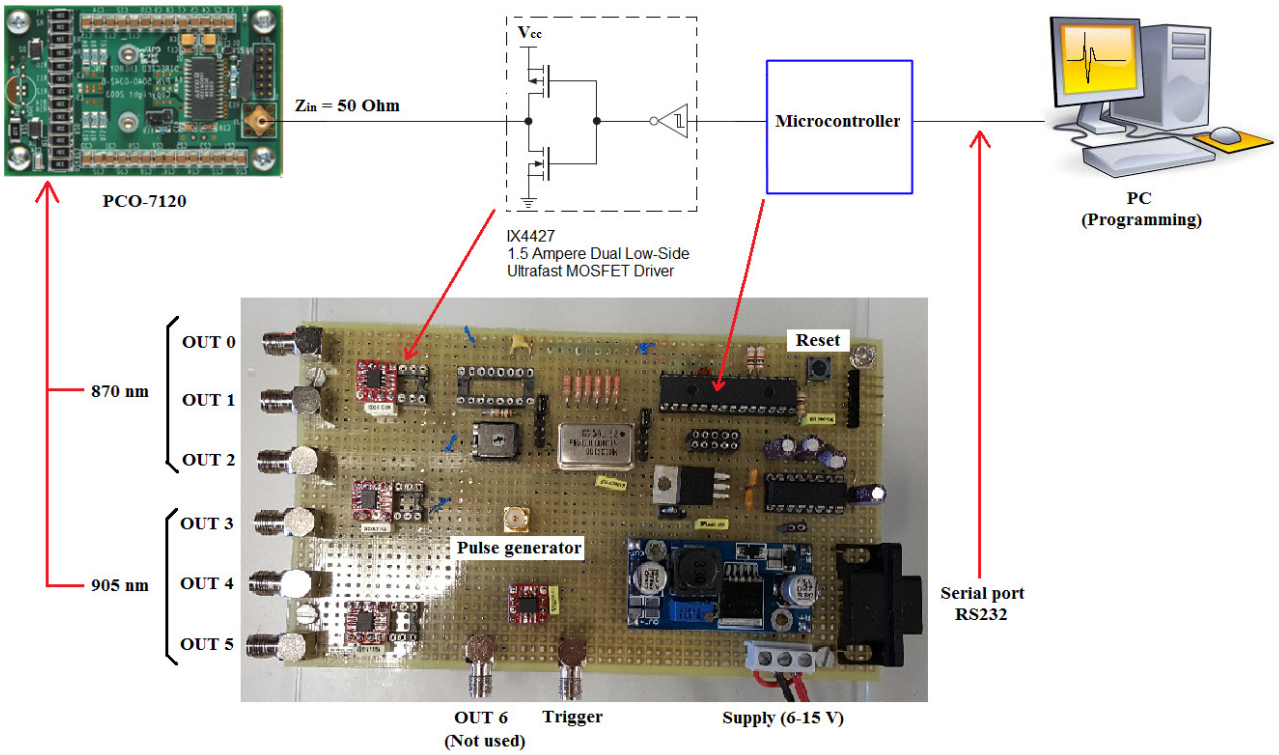


**Figure 2.** Microcontroller circuit to switch the pulse emission between the two wavelengths. This circuit can supply up to seven laser sources.

including the microcontroller circuit that is programmed from the PC by using a Matlab code. The PC sends the commands to the serial port RS232 of the circuit board. At the output of the microcontroller there is an ultrafast MOSFET driver (IX4427) that matches the output of the microcontroller (high impedance) with the input of two diode laser drivers (50 Ω each one). In addition, the ultrafast switching (a few ns) of this component ensures a very good pulse shape.

In a real OAI environment, this switching time would facilitate the fast acquisition of high-resolution images. In the next experiments, the authors switch the times between the two wavelengths for a fast estimation of the concentrations of the gold nanorods solutions, avoiding that the temperature fluctuations and the larger measurement errors that occur in a prolonged measurement time would affect the measurement accuracy.

## 2.2. Measurement Setup for OA Signal Generation

The measurement setup consists of the fiber bundle output, a cuvette holder containing a 1 cm quartz cuvette (model Z600768-1EA, Hellma GmbH) with path length of 0.4 cm, a 10-MHz piezoelectric transducer (V327-SU, Olympus Corp.), a 40-dB preamplifier, an oscilloscope, and a PC to record the OA signals (Fig. 3). The cuvette holder has four ports in total including a SMA-fiber-adapter input that has a collimator lens built-in and a modified port to accommodate the piezoelectric transducer. The OA signals generated are detected by the piezoelectric transducer and then pre-amplified of 40 dB. Afterwards, they are digitized on the oscilloscope which is synchronized with the pulse emission through the trigger generator. Finally, the OA signals are sent to a PC for recording and filtering. Each triplet of HPDLs is triggered with the same signal obtaining a complete overlapping of the optical pulses after the output of the fiber bundle. The output of the fiber bundle is collimated by an aspheric lens (N.A. = 0.22, effective focal length $f_{\mathrm{EFL}} = 12$ mm, material: D-ZK3) with anti-reflection coating (600–1050 nm) to illuminate the sample uniformly. Distilled water is used as a coupling agent between transducer and the wall of the cuvette. The average power measured at the output of the 12-mm

**Table 2.** Characteristics of the optical pulses used for generating the OA signals.

| Parameter | 870-nm HPDLs | 905-nm HPDLs |
|---|---|---|
| Pulse width | 75 ns | 75 ns |
| Repetition rate | 1 kHz | 1 kHz |
| Duty cycle | 0.0075% | 0.0075% |
| Total pulse energy | $13.56 \pm 0.022\,\mu J$ | $13.09 \pm 0.031\,\mu J$ |
| Total average power | $13.56 \pm 0.022$ mW | $13.09 \pm 0.031$ mW |
| Light spot area | $38.5\,mm^2$ | $38.5\,mm^2$ |
| Total pulse energy density | $35.2 \pm 0.06\,\mu J/cm^2$ | $34.0 \pm 0.08\,\mu J/cm^2$ |

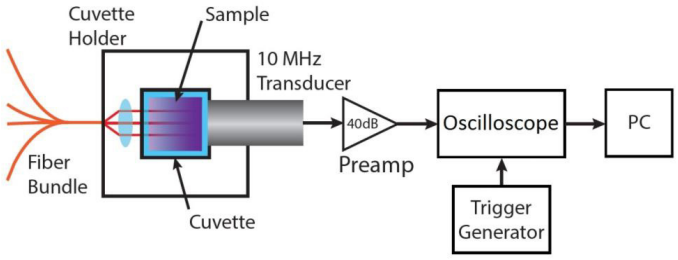


**Figure 3.** Measurement setup for the detection of OA signals.

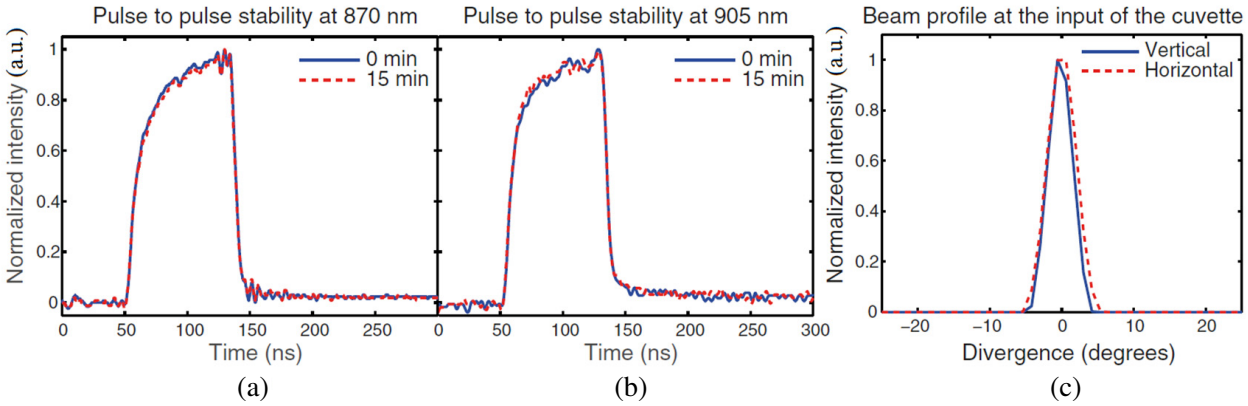


**Figure 4.** Optical pulse-to-pulse stability at: (a) 870 nm, (b) 905 nm. (c) Beam profile at the input of the cuvette.

lens, emitted by each triplet of HPDLs with a repetition frequency of 1 kHz and a pulse width of 75 ns, is $\sim 13.56 \pm 0.022$ mW and $\sim 13.09 \pm 0.031$ mW at 870 nm and 905 nm, respectively. Assuming rectangular pulses, the total pulse energies provided to the gold nanorods solutions chosen as samples are $\sim 13.56 \pm 0.022\,\mu J$ and $\sim 13.09 \pm 0.031\,\mu J$ at 870 nm and 905 nm, respectively. The beam diameter is 7 mm (spot area of $\sim 38.5\,mm^2$) in both cases. For this reason, the authors have located the 1-cm side of the cuvette perpendicular to the propagation axis for the OA measurements. Accordingly, the respective total pulse energy densities are $\sim 35.2 \pm 0.022\,\mu J/cm^2$ and $\sim 34 \pm 0.031\,\mu J/cm^2$. Table 2 reports the characteristics of the optical pulses used for excitation of OA signals at 870 nm and 905 nm, respectively.

The optical pulse-to-pulse stability has been checked at the output of the fiber bundle prior to experiments, showing unchanged characteristics at each wavelength in a period of 15 minutes (Figs. 4(a) and (b)). Fig. 4(c) shows the beam profile at the input of the cuvette. The uniform illumination of the

sample is achieved between vertical and horizontal axes.

In addition, the automatization of the measurements provided by the microcontroller circuit avoids manipulating the system for every single step, maintaining the alignment between the source, the sample and the piezoelectric transducer. In this line, the accuracy of the measurements is maintained accurate.

## 3. CHARACTERIZATION OF GOLD NANORODS

In this section the characteristics of the gold nanorods solutions and the algorithm for the determination of their concentrations from the detected OA signals are described.

### 3.1. Absorbance Spectra of Gold Nanorods

The authors characterized the absorbance spectra of two pure solutions of gold nanorods with absorbance peak (optical density (O.D.) = 20) at $\sim$ 860 nm and $\sim$ 900 nm, respectively, over the spectral range between 410 and 1100 nm (Fig. 5) by using a spectrophotometer (Lambda 14P, Perkin Elmer Inc.) and considering a path length of 1 cm in a fused quartz cuvette. The main characteristics of the gold nanorods are reported in Table 3. The authors call NP1 the gold nanorods with absorbance peak at $\sim$ 860 nm, and NP2 the gold nanorods with absorbance peak at $\sim$ 900 nm. The corresponding absorption coefficients at 870 nm and 905 nm, reported in Table 3 as well, can be calculated from the measured spectra (Fig. 5) using the following equation [26]:

$$\mu_{abs}\left[\text{cm}^{-1}\right] = 2.303 \times \text{O.D.}, \tag{1}$$

considering that O.D. corresponds to the absorbance using a path length of 1 cm.

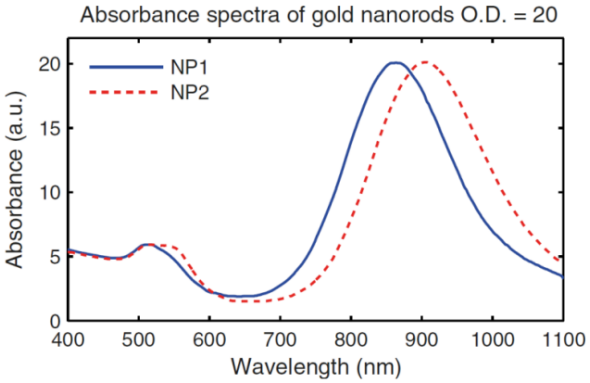


**Figure 5.** Absorbance spectra of two colloidal solutions of gold nanorods with peak at: $\sim$ 860 nm (blue line) and $\sim$ 900 nm (red dots) (O.D. = 20). The solutions have been diluted with a factor of 20 before measurements.

**Table 3.** Main characteristics of the gold nanorods samples and measured absorption coefficients at 870 nm and 905 nm.

| Characteristics | NP1 | NP2 |
|---|---|---|
| Longitudinal peak | 858 nm | 900 nm |
| Transverse peak | 513 nm | 516 nm |
| Mass concentration (Au) | 0.9 mg/ml | 0.8 mg/ml |
| $\mu_{abs}$ @ 870 nm ($\text{cm}^{-1}$) | $\sim$ 45.8 | $\sim$ 41.7 |
| $\mu_{abs}$ @ 905 nm ($\text{cm}^{-1}$) | $\sim$ 39.6 | $\sim$ 46.0 |

### 3.2. Determination of Nanoparticles Concentration Optoacoustically

In [23], an optical inverse problem has been proposed to estimate the concentrations $C_m$ of $M$ chromophores with known absorption coefficient spectra, from the 3D map of the energy absorbed in a tissue. Some parameters involved in the algorithm were considered dependent on both the wavelength $\lambda$ and position vector $\mathbf{x}$ (i.e., total absorption coefficient, absorbed energy density, and light fluence), while the concentration was considered dependent only on the position vector $\mathbf{x}$, and the known absorption coefficient dependent on the wavelength $\lambda$. In this case,the authors only consider an inverse algorithm for a 1D environment with no dependence on the position vector $\mathbf{x}$. Considering a homogeneous mixture of $M$ solutions of nanoparticles with respective concentrations $C_m$ and a set of $N$ operating wavelengths, the total absorption coefficient $\mu_{\mathrm{TOT}}(\lambda_n)\,(\mathrm{cm}^{-1})$ of the mixed solution is a function of the wavelength $\lambda_n$ and can be expressed as:

$$\mu_{\mathrm{TOT}}(\lambda_n) = \sum_{m=1}^{M} \mu_m(\lambda_n)\, C_m, \tag{2}$$

where $\mu_m(\lambda_n)$ is the known (from the spectra) absorption coefficient $(\mathrm{cm}^{-1})$ of the reference solution of nanoparticles $m$ at wavelength $\lambda_n$. Under thermal and stress confinement conditions and using a broadband ultrasonic transducer, the OA signal $V(\lambda_n)$ detected by the oscilloscope is proportional to the pressure $p(d,\lambda_n)$ that is related to the total absorption coefficient $\mu_{\mathrm{TOT}}(\lambda_n)$ by the following equation:

$$V(\lambda_n) \propto p(d,\lambda_n) = \Gamma \mu_{\mathrm{TOT}}(\lambda_n)\, \phi(d,\lambda_n), \tag{3}$$

where $d$ is the depth in the sample, $\Gamma$ a term of OA efficiency depending on intrinsic thermal effects, called *Grüneisen parameter*, and the unknown fluence can be expressed as $\phi(d,\lambda_n) = A(\lambda_n)\, e^{-\mu_{att}(\lambda_n)d}$, where $A(\lambda_n)$ is the input pulse energy and $\mu_{att}(\lambda_n)$ is the total attenuation coefficient including both absorption and scattering effects. The exponential term will be analyzed more in details afterwards. In turn, the input energy $A(\lambda_n)$ can be related to the input average power $P(\lambda_n)$ by the relation $A(\lambda_n) = kP(\lambda_n)$, where $k$ is a proportionality term (i.e., inverse of the pulse repetition rate). Additionally, it can be defined $k' = k\Gamma$. Hence, Eq. (3) can be reformulated as:

$$V(\lambda_n) = k' \mu_{TOT}(\lambda_n)\, P(\lambda_n)\, e^{-\mu_{att}(\lambda_n)d}, \tag{4}$$

Combining Eqs. (2) and (4), the following equation is obtained:

$$V(\lambda_n) = k' \sum_{m=1}^{M} \mu_m(\lambda_n)\, C_m P(\lambda_n)\, e^{-\mu_{att}(\lambda_n)d}, \tag{5}$$

In Eq. (5), the OA signals $V(\lambda_n)$ can be normalized by the input power as $B(\lambda_n) = V(\lambda_n)/(P(\lambda_n)\, e^{-\mu_{att}(\lambda_n)d})$. Hence, Eq. (5) can be expressed in an $N \times M$ matrix as follows:

$$\begin{vmatrix} B(\lambda_1) \\ B(\lambda_2) \\ \vdots \\ B(\lambda_N) \end{vmatrix} = k' \begin{bmatrix} \mu_1(\lambda_1) & \cdots & \mu_M(\lambda_1) \\ \vdots & \ddots & \vdots \\ \mu_1(\lambda_N) & \cdots & \mu_M(\lambda_N) \end{bmatrix} \begin{vmatrix} C_1 \\ C_2 \\ \vdots \\ C_M \end{vmatrix}, \tag{6}$$

The terms $B(\lambda_n)$ can be simplified considering just the signal amplitude that comes from the entrance of the cuvette, which means considering $\mu_{att}(\lambda_n)d \ll 1$. In this case, $e^{-\mu_{att}(\lambda_n)d} \approx 1$ and the system (6) becomes linear. The concentrations $C_m$ can be easily calculated inverting the matrix of absorption coefficients. This approximation presents two advantages. First, $V(\lambda_n)$ can be easily found from the peak-to-peak amplitude of the first OA signal, whose redundancy occurs at some fixed delays, depending on the speed of sound in the sample. Second, an ultra-wideband ultrasonic transducer is not required, contrary to what is commonly used in conventional OAI.

A resonant PZT transducer would behave as a band-pass filter, filtering out the lower frequencies and enhancing the OA signal that comes from the boundaries, like the first interface of the sample. In this way, the total noise present in the OA signal would be reduced, improving the sensitivity of detection.

## 4. EXPERIMENTAL VALIDATION AND RESULTS

The aim of this paper is to estimate the concentrations $C_1$ and $C_2$ of two solutions of gold nanorods (NP1 and NP2) mixed in a quartz cuvette from the evaluation of the OA signals detected at 870 nm and 905 nm. As anticipated in the introduction, three different mixtures of gold nanorods containing different percentages of the two solutions are considered: I) 40% NP1 and 60% NP2, II) 50% NP1 and 50% NP2, III) 60% NP1 and 40% NP2. The OA signals are obtained from each mixture using the dual-wavelength diode laser-based system and following the experimental setup described in Subsection 2.2. The OA signals detected for each mixture at 870 nm and 905 nm are depicted in Fig. 6 after applying a boxcar filtering. In all the signals, a noise around 0 µs can be observed, which is generated by the coupling of the diode laser current pulse into the detector amplifier, but the OA signal is not affected because it arrives at the transducer after $\sim 3$ µs. For the case of two different absorbers and two wavelengths, Eq. (6) is reduced to:

$$\begin{vmatrix} B(\lambda_1) \\ B(\lambda_2) \end{vmatrix} = \begin{bmatrix} \mu_1(\lambda_1) & \mu_2(\lambda_1) \\ \mu_1(\lambda_2) & \mu_2(\lambda_2) \end{bmatrix} \begin{vmatrix} S_1 \\ S_2 \end{vmatrix}, \tag{7}$$

where $S_m = k'C_m$, $\lambda_1 = 870$ nm and $\lambda_2 = 905$ nm. By inverting Eq. (7), it is possible to find the parameters $S_1$ and $S_2$ that contain the unknown factor $k'$. Finally, the concentrations can be obtained

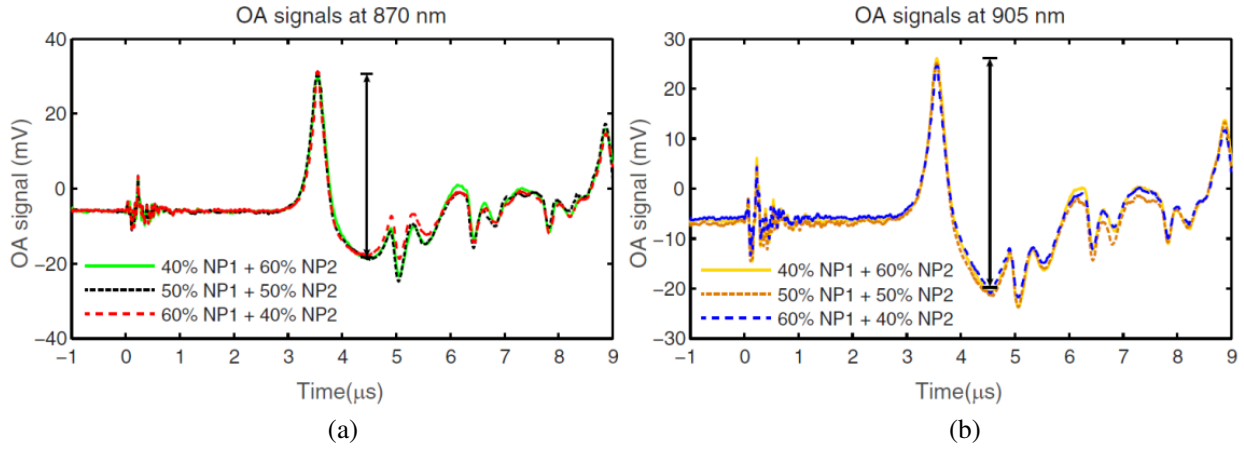


**Figure 6.** OA signals detected from three different mixtures of gold nanorods at: (a) 870 nm and (b) 905 nm. For the calculation of the concentrations of gold nanorods the authors considered their peak-to-peak amplitudes as indicated between the first maximum and the first minimum.

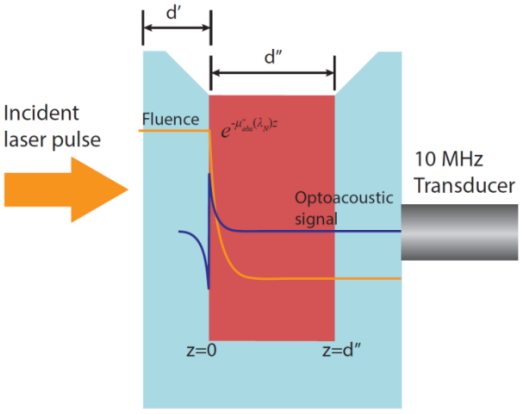


**Figure 7.** Light attenuation inside the gold nanorods hosted in a quartz cuvette and optoacoustic signal generated at the interface.

as a volume percent, knowing that the sample is a mixture exclusively of the two solutions of gold nanorods, as follows:

$$C_m(\%) = \frac{S_m}{S_1 + S_2} \times 100, \tag{8}$$

As mentioned before, the term $B(\lambda_n)$ corresponds to the peak-to-peak amplitude of the first OA pulse arriving to the ultrasonic transducer, normalized by the optical energy that reaches the cuvette at each wavelength. The quartz cuvette employed is transparent and its transmission coefficient does not vary significantly between the two wavelengths considered. Thus, the OA signal is totally produced by the sample hosted inside the cuvette.

The amount of time (called "time of flight" (TOF)) required by the OA signal to reach the transducer from the cuvette-sample interface (Fig. 7) is given by the following equation:

$$\mathrm{TOF} = d'\nu_C + d''\nu_S, \tag{9}$$

where $d'$ is the thickness of the cuvette wall, $v_C$ the speed of sound in the quartz cuvette, $d''$ the thickness of the cuvette hole, and $v_S$ the speed of sound in the sample. Due to the acoustic impedance mismatch between the sample and the cuvette and between the cuvette and the surrounding air, a series of reverberations occurs after the arrival of the first maximum. The detection of the OA signals mostly depends on the bandwidth of the piezoelectric transducer. To improve the accuracy of the measurements and properly detect the amplitude of the OA signals, the transducer should be wideband or at least have a central frequency high enough to avoid the overlapping of the reverberations of the OA signal in the walls of the cuvette. The quartz cuvette employed in the experiments has a wall thickness $d'$ equal to 3 mm, so the reflections are expected every $\sim 1.39\,\mu$s after the first OA signal peak, as shown in Fig. 6. A transducer of 10 MHz is used to ensure that each reflection is individually resolved. Furthermore, if the transducer had a lower bandwidth (i.e., 1 MHz) the OA signal would be truncated and it would not be got the correct amplitude when the absorber exhibits high absorption coefficient [23]. The peak-to-peak amplitude from the first maximum to the next minimum, measured as indicated in Fig. 6, is averaged over 10 measurements and is reported in Table 4. Taking into account the signal averaging, the total time required for the measurement of the amplitudes at both wavelengths was 10 ms.

Finally, the single concentrations of the gold nanorods composing the mixtures, shown in Table 5, are estimated from the OA signal amplitudes reported in Table 4, after being normalized by the pulse energy at the corresponding wavelength (Table 2), by using Eqs. (7) and (8). The calculated values of $C_1$ and $C_2$ are reported in mean value and standard deviation and present a maximum divergence of 2.76% from the expected values. This observational error is compatible with the digitizing error of the 8-bit oscilloscope employed for measuring the signals.

**Table 4.** Peak-to-peak OA signals at 870 nm and 905 nm after boxcar filtering in Matlab.

| | **Optoacoustic signal (mV)** | | |
|---|---|---|---|
| **Wavelength** | **40% NP1 60% NP2** | **50% NP1 50% NP2** | **60% NP1 40% NP2** |
| 870 nm | $48.6 \pm 0.1$ | $49.2 \pm 0.1$ | $49.9 \pm 0.1$ |
| 905 nm | $46.8 \pm 0.1$ | $46.6 \pm 0.1$ | $46.3 \pm 0.1$ |

**Table 5.** Values of the gold nanorods concentrations estimated from the OA signals measured.

| | **Estimated concentrations (%)** | | | | | |
|---|---|---|---|---|---|---|
| **Nanoparticles** | **40% NP1 60% NP2** | | **50% NP1 50% NP2** | | **60% NP1 40% NP2** | |
| **$C_1$: NP1** | 41.97 | $\pm 1.06$ | 48.79 | $\pm 1.05$ | 57.24 | $\pm 1.04$ |
| **$C_2$: NP2** | 58.03 | | 51.21 | | 42.76 | |

## 5. CONCLUSIONS

A microcontroller circuit has been implemented to provide fast wavelength switching between 870 nm and 905 nm with the aim to generate OA signals from several mixtures of gold nanorods solutions with different absorbance peaks. The concentrations of these solutions have been estimated with very high accuracy from the amplitudes of the OA signals detected. The results achieved show that the concentrations of gold nanorods are measured with acceptable observational error from the real values, and it is also due to the fast wavelength switching provided by the microcontroller circuit. The gold nanorods presented could have a role of contrast agents in real OA applications aimed at the detection of diseases, due to their high absorbance and biocompatibility. In a real OAI scenario, the real-time monitoring of the concentrations of gold nanoparticles can be useful to know the quantity that should be administered to have appreciable contrast between the interested chromophores. Future research on this field will be addressed to add new NIR wavelengths to the OA system (such as 808 nm, 940 nm, and 980 nm) for potential applications in multi-spectral OAI. Actually, working in a larger range of wavelengths will allow a better differentiation between chromophores during the image processing. The requirements of high power to penetrate deeply into biological tissues can be fulfilled using diode laser bars emitting several hundreds of Watts of peak power.

## ACKNOWLEDGMENT

We acknowledge the support from DIFRAGEOS project (P2013/ICE-3004), funded by the Consejería de Educación, Juventud y Deporte of Comunidad de Madrid.

## DISCLOSURE

The authors have no financial interests in the manuscript. There are no potential conflicts of interest to declare.

## REFERENCES

1. Xu, M. H. and L. V. Wang, "Photoacoustic imaging in biomedicine," *Review of Scientific Instruments*, Vol. 77, No. 4, 041101, 2006.
2. Xia, J., J. Yao, and L. V. Wang, "Photoacoustic tomography: principles and advances," *Progress In Electromagnetics Research*, Vol. 147, 1–22, 2014.
3. Beard, P. C., "Biomedical photoacoustic imaging," *Interface Focus*, Vol. 1, No. 4, 602–631, 2011.
4. Gusev, V. Ė. and A. A. Karabutov, *Laser Optoacoustics*, American Institute of Physics, New York, 1993.
5. Li, C. H. and L. V. Wang, "Photoacoustic tomography and sensing in biomedicine," *Physics in Medicine and Biology*, Vol. 54, No. 19, R59–R97, 2009.
6. Lee, J., Y. J. Lee, E. J. Jeong, M. Y. Jung, S. Lee, B. K. Kim, and D. H. Song, "Gain-switched Ti:sapphire laser-based photoacoustic imaging," *Applied Optics*, Vol. 55, No. 20, 5419-22, 2016.
7. Upputuri, P. K. and M. Pramanik, "Performance characterization of low-cost, high-speed, portable pulsed laser diode photoacoustic tomography (PLD-PAT) system," *Biomedical Optics Express*, Vol. 6, No. 10, 4118–4129, 2015.
8. Friedrich, C. S., M. C. Wawreczko, M. P. Mienkina, N. C. Gerhardt, G. Schmitz, and M. R. Hofmann, "Compact semiconductor laser sources for photoacoustic imaging," *Proceedings of SPIE*, Vol. 7177, 71772H, 2009.
9. Talele, K. and D. S. Patil, "Analysis of wave function, energy and transmission coefficients in GaN/ALGaN superlattice nanostructures," *Progress In Electromagnetics Research*, Vol. 81, 237–252, 2008.
10. Sonawane, U. S., E. P. Samuel, C. K. Kasar, and D. S.Patil, "Nanosimulation of electron confinement in cerium doped zinc oxide nanowire structure for light emitting devices," *Optik*, Vol. 127, No. 12, 4937–4940, 2016.

11. Patil, D. S. and D. K. Gautam, "Computer analysis and optimization of physical and material parameters of the blue laser diode," *Optics Communications*, Vol. 201, Nos. 4–6, 413–423, 2002.
12. Allen, T. J. and P. C. Beard, "Pulsed near-infrared laser diode excitation system for biomedical photoacoustic imaging," *Optics Letters*, Vol. 31, No. 23, 3462–3464, 2006.
13. Zeng, L. M., G. D. Liu, D. W. Yang, and X. R. Ji, "Portable optical-resolution photoacoustic microscopy with a pulsed laser diode excitation," *Applied Physics Letters*, Vol. 102, No. 5, 053704, 2013.
14. Wang, T. H., S. Nandy, H. S. Salehi, P. D. Kumavor, and Q. Zhu, "A low-cost photoacoustic microscopy system with a laser diode excitation," *Biomedical Optics Express*, Vol. 5, No. 9, 3053–3058, 2014.
15. Allen, T. J. and P. C. Beard, "Dual wavelength laser diode excitation source for 2D photoacoustic imaging," *Proceedings of SPIE*, Vol. 6437, 64371U, 2007.
16. Kolkman, R. G. M., W. Steenbergen, and T. G. van Leeuwen, "In vivo photoacoustic imaging of blood vessels with a pulsed laser diode," *Lasers in Medical Science*, Vol. 21, No. 3, 134–139, 2006.
17. Zeng, L. M., G. D. Liu, D. W. Yang, and X. R. Ji, "3D-visual laser-diode-based photoacoustic imaging," *Optics Express*, Vol. 20, No. 2, 1237–1246, 2012.
18. Hempel, M., J. W. Tomm, F. La Mattina, I. Ratschinski, M. Schade, I. Shorubalko, M. Stiefel, H. S. Leipner, F. M. Kießling, and T. Elsaesser, "Microscopic origins of catastrophic optical damage in diode lasers," *IEEE Journal of Selected Topics in Quantum Electronics*, Vol. 19, No. 4, 1500508, 2013.
19. Leggio, L., D. C. Gallego, S. B. Gawali, E. Dadrasnia, M. Sánchez, S. Rodríguez, M. González, G. Carpintero, M. Osiński, and H. Lamela, "Optoacoustic response from graphene-based solutions embedded in optical phantoms by using 905-nm high-power diode-laser assemblies," *Proceedings of SPIE*, Vol. 9708, 97083M, 2016.
20. Zhang, H. F., K. Maslov, M. Sivaramakrishnan, G. Stoica, and L. V. Wang, "Imaging of hemoglobin oxygen saturation variations in single vessels in vivo using photoacoustic microscopy," *Applied Physics Letters*, Vol. 90, No. 5, 053901-3, 2007.
21. Andree, S., J. Helfmann, and I. Gersonde, "Determination of chromophore concentrations from spatially resolved skin measurements," *Proceedings of SPIE*, Vol. 8087, 808716, 2011.
22. Laufer, J. G., B. Cox, E. Zhang, and P. C. Beard, "Quantitative determination of chromophore concentrations from 2D photoacoustic images using a nonlinear model-based inversion scheme," *Applied Optics*, Vol. 49, No. 8, 1219-33, 2010.
23. Cox, B., J. G. Laufer, S. Arridge, and P. C. Beard, "Quantitative spectroscopic photoacoustic imaging: a review," *Journal of Biomedical Optics*, Vol. 17, No. 6, 061202, 2012.
24. Lin, A. W., N. A. Lewinski, J. L. West, N. J. Halas, and R. A. Drezek, "Optically tunable nanoparticle contrast agents for early contrast agents for early cancer detection: model-based analysis of gold nanoshells," *Journal of Biomedical Optics*, Vol. 10, No. 6, 064035, 2005.
25. Cunningham, V., H. Lamela, and D. C. Gallego, "Laser optoacoustic scheme for highly accurate characterization of gold nanostructures in liquid phantoms for biomedical applications," *Journal of Nanophotonics*, Vol. 7, No. 1, 073078, 2013.
26. Li, W. and X. Chen, "Gold nanoparticles for photoacoustic imaging," *Nanomedicine*, Vol. 10, No. 2, 299–320, 2015.
27. Wang, L. V., *Photoacoustic Imaging and Spectroscopy*, CRC Press Eds., Boca Raton, Florida, 2009.